12-1-2008

Modeling and simulation of field-effect biosensors (BioFETs) and their deployment on the nanoHUB

Clemens Heitzinger
Wolfgang Pauli Institute - University of Vienna

Rick Kennell
Purdue University - Main Campus

Gerhard Klimeck
Purdue University - Main Campus, gekco@purdue.edu

Norbert Mauser
Wolfgang Pauli Institute - University of Vienna

Michael McLennan
Purdue University -0 Main Campus

See next page for additional authors

Authors
Clemens Heitzinger, Rick Kennell, Gerhard Klimeck, Norbert Mauser, Michael McLennan, and Christian Ringhofer

Journal of Physics: Conference Series **107** (2008) 012004 doi:10.1088/1742-6596/107/1/012004

Modeling and simulation of field-effect biosensors (BioFETs) and their deployment on the nanoHUB

Clemens Heitzinger,[1] Rick Kennell,[2] Gerhard Klimeck,[2] Norbert Mauser,[1] Michael McLennan,[2] and Christian Ringhofer[1,3]

[1] Wolfgang Pauli Institute c/o Faculty of Mathematics, University of Vienna, A–1090 Vienna, Austria
[2] School of Electrical and Computer Engineering, Purdue University, West Lafayette, IN 47907, USA
[3] Department of Mathematics, Arizona State University, Tempe, AZ 85287, USA

E-mail: Clemens.Heitzinger@univie.ac.at

Abstract. BioFETs (biologically active field-effect transistors) are biosensors with a semiconductor transducer. Due to recent experiments demonstrating detection by a field effect, they have gained attention as potentially fast, reliable, and low-cost biosensors for a wide range of applications. Their advantages compared to other technologies are direct, label-free, ultra-sensitive, and (near) real-time operation. We have developed 2D and 3D multi-scale models for planar sensor structures and for nanowire sensors. The multi-scale models are indispensable due to the large difference in the characteristic length scales of the biosensors: the charge distribution in the biofunctionalized surface layer varies on the Angstrom length scale, the diameters of the nanowires are several nanometers, and the sensor lengths measure several micrometers. The multi-scale models for the electrostatic potential can be coupled to any charge transport model of the transducer. Conductance simulations of nanowire sensors with different diameters provide numerical evidence for the importance of the dipole moment of the biofunctionalized surface layer in addition to its surface charge. We have also developed a web interface to our simulators, so that other researchers can access them at the nanoHUB and perform their own investigations.

1. Introduction

The basic idea of field-effect biosensors (BioFETs, biologically active field-effect transistors) stems from the ion-selective field-effect transistor (ISFET). In ISFETs, the gate of a MOSFET (metal-oxide-semiconductor field-effect transistor) is replaced by an ion-selective layer, an aqueous solution, and a reference electrode [1–3]. Such devices measure the concentrations of certain ion species in the liquid and therefore act as pH sensors. More recently, biosensors like EnFETs (enzyme FETs), ImmunoFETs, and DNAFETs were devised building upon the ISFET concept by replacing the ion-selective layer of ISFETs by layers of immobilized enzymes, antibodies, or DNA strands [4–6].

All of these devices are BioFETs (see Fig. 1). Whereas a traditional field-effect transistor (FET) uses a gate contact to control the conductance of the semiconductor between its source and drain contacts, a BioFET replaces the gate structure by a biofunctionalized layer of immobilized probe molecules that act as surface receptors. When matching target molecules bind to the receptors,

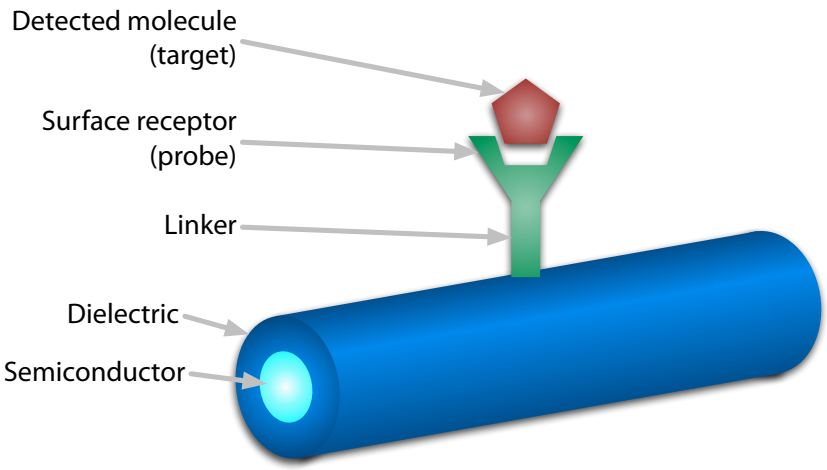

Figure 1. Schematic diagram of a silicon-nanowire BioFET. The linkers, the surface receptors (antibodies or single-stranded DNA or PNA oligomers), and possibly the target molecules (antigens or the complementary single-stranded DNA or PNA oligomers) are repeated along the nanowire. The conductance of the nanowire is measured between the 'source' and 'drain' contacts on the left and on the right.

the charge distribution in the boundary layer at the liquid-transducer interface of the device changes. Hence this modulation of the conductance of the transducer enables detection.

The advantages of BioFETs compared to optical methods are direct, label-free, (near) real-time, continuous, and highly selective sensing. In fact their selectivity can be called perfect, since binding between an antibody and an antigen (i.e., the probe and target molecules) is equivalent to having an immunological or biological function. The concept of field-effect sensors is very appealing, since it is known how to functionalize silica surfaces to detect virtually all biomolecules: for DNA and RNA detection, PNA (peptide nucleic acid) probe molecules are used; for the detection of other biomolecules, suitable monoclonal antibodies are used (which are commercially available for many biomolecules). Therefore the BioFET is a very general concept for the detection of molecules in liquids. Hence possible applications of BioFETs, possibly arranged in arrays, are the detection of tumor markers, the detection of SNPs (single-nucleotide polymorphisms, or point mutations) and polymorphisms in general.

First experiments with conventional (flat MOSFET) structures were reported in [7, 8]. More recently, silicon nanowires were used as transducers [9–14]. Their advantage is a higher surface-to-volume ratio and thus an increased modulation of the conductance by the biomolecules. Despite the recent experimental advances, the functioning of these field-effect devices is not well understood [5, 6].

In Section 2, our models for BioFET simulation are described. The most important part is a theorem stating how the fast-varying charge distribution in the boundary layer at the liquid-transducer interface can be replaced by equivalent interface conditions. Simulation results and their implications are discussed in Section 3. The deployment of BioFET simulators on the nanoHUB is described in Section 4. Finally, we close with the conclusions in Section 5.

2. BioFET models

A quantitative theory of the functioning of BioFETs has not been developed previously. Experimental work has not been accompanied by models or simulations, and BioFET models were adaptations of ISFET models, mostly neglecting the precise structure and charge distribution in

the biofunctionalized layer. Also in the history of ISFET modeling, the capacity of the surface layer proved to be an important but difficult point, even in the absence of biomolecules.

BioFET models are complicated by two facts. First, in order to quantitatively explain the field effect, all charges in the system must obviously be taken into account in a self-consistent manner. Second, the structure and charge distribution in the biomolecules in the surface layer varies on the Angstrom length scale, whereas the sensor sizes are in the micrometer range. In experiments with conventional flat structures, the exposed sensor areas measured several micrometers, and also the nanowire sensors are several micrometers long with diameters down to approximately 5nm. We have solved this multi-scale problem by homogenization as described below. Therefore the multi-scale model presented here is the fundamental part of the model that bridges the different length scales and enables self-consistent simulation.

In previous work we focused on different aspects of the devices [15–20]. The details of the multi-scale models and the homogenization, including proofs, can be found in [21, 22].

2.1. The model equations

We first describe the model equations for the electric potential in a nanoplate BioFET [21]. The device consists of several layers: at the bottom is the back gate or bulk contact; there is an optional silicon-oxide layer, if a silicon-on-insulator device is considered; the transducer is a silicon nanoplate; the interface to the liquid is given by a silicon-oxide layer; on top of the silicon oxide there is the biofunctionalized surface layer containing the probe and target molecules in the liquid; then there is the bulk liquid; and finally on top there is an electrode.

Now we introduce the 3D coordinate system for the simulation domain containing a nanoplate BioFET. The origin of the coordinate system is on the source contact and the interface between the sensor and the liquid containing the analyte; the positive x-axis points into the semiconductor; the negative x-axis points into the liquid; the positive y_1-axis points towards the drain contact which starts at $y_1 = L_1$; and the y_2-axis is normal to the x- and y_1-axes.

The basic model equation is the mean-field Poisson equation

$$-\partial_x\big(\epsilon(x)\partial_x V(x,\mathbf{y})\big) - \nabla_{\mathbf{y}}\cdot\big(\epsilon(x)\nabla_{\mathbf{y}} V(x,\mathbf{y})\big) = n_T\big(V(x,\mathbf{y}),x,\mathbf{y}\big) + n_E(x,\mathbf{y}) =: n(x,\mathbf{y}) \qquad (1)$$

where $x \in \mathbb{R}$, $\mathbf{y} = (y_1, y_2) \in [0, L_1] \times [0, L_2] =: L$, V is the electrostatic potential, and ϵ is the permittivity. Here n denotes the charge density in the semiconductor and in the dielectric layer (for $x > 0$) and in the liquid (for $x < 0$). The charge density consists of two parts, namely a self-consistent part n_T providing the connection to an arbitrary charge transport model and a given set of external, fixed charges n_E.

In the liquid ($x < 0$), ions are mobile charge carriers which are modeled by a Boltzmann model of the form

$$n_T\big(V(x,\mathbf{y}),x,\mathbf{y}\big) := \sum_{\sigma\in E} \sigma f_\sigma(x,\mathbf{y}) \mathrm{e}^{-\sigma\beta V(x,\mathbf{y})}, \qquad (2)$$

where the functions f_σ are given by the exponentials of the chemical potentials $\Phi_\sigma(x,\mathbf{y})$, i.e., $f_\sigma(x,\mathbf{y}) = \mathrm{e}^{\sigma\beta\Phi_\sigma(x,\mathbf{y})}$ holds. Here q is the elementary (proton) charge, k is the Boltzmann constant, T denotes the temperature, $\beta := q/(kT)$, and E denotes the types of charges present in the liquid as dimensionless multiples of the elementary charge. In the liquid, the most common example is $E := \{-1, +1\}$ corresponding to a 1:1 electrolyte. The system (1), (2) is known as the Poisson-Boltzmann equation in computational chemistry and arises in Debye-Hückel theory [23–25].

For the semiconductor ($x > 0$) the most popular model is the drift-diffusion model [26], where the total charge density n_T is given, in steady-state, as the solution of a set of elliptic diffusion-convection equations.

Furthermore the permittivity ϵ is the piecewise constant function

$$\epsilon(x) := \begin{cases} \epsilon_- \in \mathbb{R} & \text{for } x < 0 \\ \epsilon_+ \in \mathbb{R} & \text{for } x > 0. \end{cases}$$

Therefore there are two conditions for the interface $x = 0$, namely the continuity of the potential and the continuity of the electric displacement,

$$V(0-, \mathbf{y}) = V(0+, \mathbf{y}), \tag{3a}$$
$$\epsilon_- \partial_x V(0-, \mathbf{y}) = \epsilon_+ \partial_x V(0+, \mathbf{y}). \tag{3b}$$

In the semiconductor ($x > 0$), the external charges n_E in (1) are given by the background density of impurity ions, i.e., the doping of the semiconductor. In the liquid ($x < 0$), the external charges are given by the partial charges of the biomolecules and the ions in the surface layer. Hence we have

$$n_E(x, \mathbf{y}) := \begin{cases} \rho(x, \mathbf{y}) & \text{for } x < 0 \\ n_+(x, \mathbf{y}) & \text{for } x > 0 \end{cases}$$

with n_+ being the doping concentration of the semiconductor and ρ being the charge density of the surface or boundary layer.

The problem that must be solved is a homogenization problem, since in the surface or boundary layer the charge density ρ exhibits a spatial structure which cannot be resolved within a self-consistent charge transport model. The grid would have to be much too fine. Our goal was to replace the problem (1) by a homogenized problem, consisting of a transport model in the semiconductor and the liquid and including interface conditions that describe the effect of the surface layer charges. Before we can summarize the result of the homogenization [21], we have to make a few definitions for the surface layer.

2.2. The fine structure of the biofunctionalized layer

To resolve the fine structure of the biofunctionalized surface (or boundary) layer, we divide it into cells. Each cell can contain either a probe molecule or a probe and target molecule complex. Therefore we divide the interface into $N_1 \times N_2$ periodically repeated cells and define

$$\mathbf{m} := \begin{pmatrix} m_1 L_1 \\ m_2 L_2 \end{pmatrix} \quad \text{for } m_1, m_2 \in \mathbb{Z}$$

and

$$\mathcal{C}_{\mathbf{m}} := \big[(m_1 - 1)\lambda L_1, m_1 \lambda L_1\big) \times \big[(m_2 - 1)\lambda L_2, m_2 \lambda L_2\big) \quad \text{for } m_1, m_2 \in \mathbb{Z}.$$

We set $N_1 := \lceil 1/\lambda \rceil$ and $N_2 := \lceil 1/\lambda \rceil$, and note that the cells $C_{\mathbf{m}}$ are of size $\lambda L_1 \times \lambda L_2$ so that they cover the surface $[0, L_1) \times [0, L_2)$, where $\lambda \ll 1$ denotes the ratio of the spatial scale of the biomolecules to the scale of the semiconductor transport picture.

Near the interface the Poisson equation (1) shows boundary layer behavior. We can zoom into the interface by introducing local coordinates, i.e., we stretch the x- and $\mathbf{y}$-coordinates by a factor of $1/\lambda$. Hence we use the fast variables $\frac{1}{\lambda}x$ and $\frac{1}{\lambda}\mathbf{y}$ in contrast to the slow variables x and $\mathbf{y}$. We make a multi-scale ansatz by writing the charge density in the liquid ($x < 0$) with a slow and a fast variable in $\mathbf{y}$ as

$$\rho(x, \mathbf{y}) = \hat{\rho}\left(\frac{x}{\lambda}, \frac{1}{\lambda}\mathbf{y}, \mathbf{y}\right) \tag{4}$$

and by writing the functions f_σ as the sum of a homogenized solution plus a boundary layer term,

$$f_\sigma(x, \mathbf{y}) = \tilde{f}_\sigma(x, \mathbf{y}) + \hat{f}_\sigma\left(\frac{x}{\lambda}, \frac{1}{\lambda}\mathbf{y}, \mathbf{y}\right). \tag{5}$$

For simplicity we denote $\hat{\rho}$ by ρ as well. Since the cells are repeated on the surface, the functions $\rho(\xi, \boldsymbol{\eta}, \mathbf{y})$ and $\hat{f}_\sigma(\xi, \boldsymbol{\eta}, \mathbf{y})$ are periodic in $\boldsymbol{\eta}$, i.e.,

$$\rho(\xi, \boldsymbol{\eta} + \mathbf{m}, \mathbf{y}) = \rho(\xi, \boldsymbol{\eta}, \mathbf{y}) \qquad \forall m_1 \in \{0, \ldots, N_1 - 1\}, \quad \forall m_2 \in \{0, \ldots, N_2 - 1\}.$$

Furthermore $\rho(\xi, \boldsymbol{\eta}, \mathbf{y})$ decays to zero for $\xi \to -\infty$, i.e., the charges are concentrated close to the surface layer in the liquid. Now $\rho(\xi, \boldsymbol{\eta}, \mathbf{y})$ is a slowly varying function of ξ and $\boldsymbol{\eta}$. The same argument applies to $\hat{f}_\sigma$.

It will be found that the interface conditions depend on two values: the macroscopic charge density and the macroscopic dipole moment density.

Definition 1 (Macroscopic charge density)**.** *Let ρ be an L^1 function. Then the macroscopic charge density $C(\mathbf{y})$ is defined as*

$$C(\mathbf{y}) := \frac{\lambda}{L_1 L_2} \int_L \int_{\mathbb{R}^-} \rho(\xi, \boldsymbol{\eta}, \mathbf{y}) \mathrm{d}\xi \mathrm{d}\boldsymbol{\eta}. \tag{6}$$

This definition yields $C := \int_L C(\mathbf{y}) \mathrm{d}\mathbf{y}$ as the total (surface) charge. We will also consider the case of essentially neutral biomolecules which, however, possess internal partial charges summing up to zero. In this case we will have to consider dipole distributions in the limit $\lambda \to 0$.

Definition 2 (Macroscopic dipole moment density)**.** *Let ρ be an L^1 function. The macroscopic dipole moment $D(\mathbf{y})$ is defined as*

$$D(\mathbf{y}) := \begin{pmatrix} D_x(\mathbf{y}) \\ D_{\mathbf{y}}(\mathbf{y}) \end{pmatrix} := -\frac{\lambda^2}{L_1 L_2} \int_L \int_{\mathbb{R}^-} \begin{pmatrix} \xi \\ \boldsymbol{\eta} \end{pmatrix} \rho(\xi, \boldsymbol{\eta}, \mathbf{y}) \mathrm{d}\xi \mathrm{d}\boldsymbol{\eta}. \tag{7}$$

The dipole moment is defined with a minus sign, since the solution domain is defined for negative ξ. $D(\mathbf{y})$ has a factor λ^2, while $C(\mathbf{y})$ has a factor λ. Therefore the dipole moment is a higher-order effect, except when C vanishes.

2.3. The multi-scale model

After the definitions and the summary of the physical situation, we can now state the main result for the limiting problem for $\lambda \to 0$ in the fine structure of the biofunctionalized layer. The main result is the following theorem, which states that, on the macroscopic scale, the effect of the microscopic charge distribution is felt only through the surface charge density C and the dipole moment density D_x of the charge distribution defined in Definition 1 and Definition 2. They enter into the macroscopic (homogenized) model via interface conditions for the homogenized potential V_h.

Theorem 1. *Let the assumptions and definitions of the previous section hold. If the solution V of the boundary value problem*

$$-\partial_x\big(\epsilon(x)\partial_x V(x, \mathbf{y})\big) - \nabla_{\mathbf{y}} \cdot \big(\epsilon(x)\nabla_{\mathbf{y}} V(x, \mathbf{y})\big) = \sum_{\sigma \in E} \sigma f_\sigma(x, \mathbf{y}) \mathrm{e}^{-\sigma\beta V(x, \mathbf{y})} + n_E(x, \mathbf{y}), \tag{8a}$$

$$V(0-, \mathbf{y}) = V(0+, \mathbf{y}), \tag{8b}$$

$$\epsilon_- \partial_x V(0-, \mathbf{y}) = \epsilon_+ \partial_x V(0+, \mathbf{y}) \tag{8c}$$

($x \in \mathbb{R}$, $\mathbf{y} \in L$) converges weakly to a solution V_h for $\lambda \to 0$ and if

$$\lim_{\lambda \to 0} \int_L \int_{x<0} \psi(x, \mathbf{y}) \sum_{\sigma \in E} \sigma \hat{f}_\sigma \left(\frac{\epsilon_-}{\epsilon_+ \lambda} x, \frac{1}{\lambda} \mathbf{y}, \mathbf{y} \right) \mathrm{e}^{-\sigma\beta V_h(x, \mathbf{y})} \mathrm{d}x \mathrm{d}\mathbf{y} = 0$$

holds for all $\psi \in \mathcal{S}(\mathbb{R}^- \times L)$*, then* V_h *satisfies the homogenized problem*

$$-\epsilon_- \partial_x^2 V_h(x,\mathbf{y}) - \epsilon_- \Delta_{\mathbf{y}} V_h(x,\mathbf{y}) - \sum_{\sigma\in E} \sigma \tilde{f}_\sigma(x,\mathbf{y}) \mathrm{e}^{-\sigma\beta V_h(x,\mathbf{y})} = 0 \qquad \textit{for } x<0, \tag{9a}$$

$$-\epsilon_+ \partial_x^2 V_h(x,\mathbf{y}) - \epsilon_+ \Delta_{\mathbf{y}} V_h(x,\mathbf{y}) - \sum_{\sigma\in E} \sigma f_\sigma(x,\mathbf{y}) \mathrm{e}^{-\sigma\beta V_h(x,\mathbf{y})} = n_+(x,\mathbf{y}) \quad \textit{for } x>0 \tag{9b}$$

with the interface conditions

$$V_h(0+,\mathbf{y}) - V_h(0-,\mathbf{y}) = -\frac{1}{\epsilon_-} D_x(\mathbf{y}), \tag{10a}$$

$$\epsilon_+ \partial_x V_h(0+,\mathbf{y}) - \epsilon_- \partial_x V_h(0-,\mathbf{y}) = -C(\mathbf{y}). \tag{10b}$$

This is Corollary 1 from [21], where the assumptions are stated in detail. A generalization has been proved for nanowire (instead of planar) structures in [22].

This result means that the multi-scale problem of modeling the quasi-periodic biofunctionalized boundary layer by the Poisson-Boltzmann equation is solved by the Poisson-Boltzmann equation (9) in conjunction with the interface conditions (10). The influence of the atomic structure of the boundary layer and its partial charges is replaced by the interface conditions. The limiting problem can have nonlinear interface conditions (for details see [21] or [22]). The interface surface charge density C causes a jump in the field and the dipole moment density D_x causes a jump in the potential.

The multi-scale model, i.e., the interface conditions derived by homogenization, can be coupled to an arbitrary charge transport model (under certain assumptions that are fulfilled for all known semiconductor charge transport models).

3. Results and discussion

To understand the physics of nanowire BioFETs, we apply our multi-scale model to silicon nanowire sensors. The main question is, if conductance changes can be attributed to the field-effect of target molecules. The charge transport model used here is the drift-diffusion model [26] in a Scharfetter-Gummel finite-volume discretization in cylindrical coordinates with a rotational symmetry [22].

If we compare biosensor simulation to classical self-consistent semiconductor device simulation, in device simulation the boundary conditions at the gate contact are Dirichlet boundary conditions. In sensor simulation the modeling is more complicated; the electrode in the liquid is modeled by Dirichlet boundary conditions as well, but the boundary layer at the transducer-liquid interface results in interface conditions.

In [27] silicon nanowires with diameters from 5nm to 50nm and lengths from 1μm to 1000μm were used and the relative resistance change after binding of target DNA strands was measured, where a maximum resistance increase of 250% was observed. Several important variables of the biofunctionalized layer have never been characterized in the recently published experiments with nanowire sensors. Proper characterizations of, e.g., the probe spacing, the electric double layer, the counter-ions, and the orientations of the probe and target molecules entail separate research projects each and we will report our results elsewhere. Here we hence investigate the conductance of the transducers as a function of C and D_r.

Our mathematical analysis of the influence of the boundary layer in the previous section has shown that the conductance of the transducer depends on a higher-order parameter, namely the dipole moment of the biofunctionalized layer, in addition to its surface charge C. It can be argued that the total charge C of the cells in the biofunctionalized layer must vanish due to the presence of counter-ions around the biomolecules and a reconfiguration of the electric double

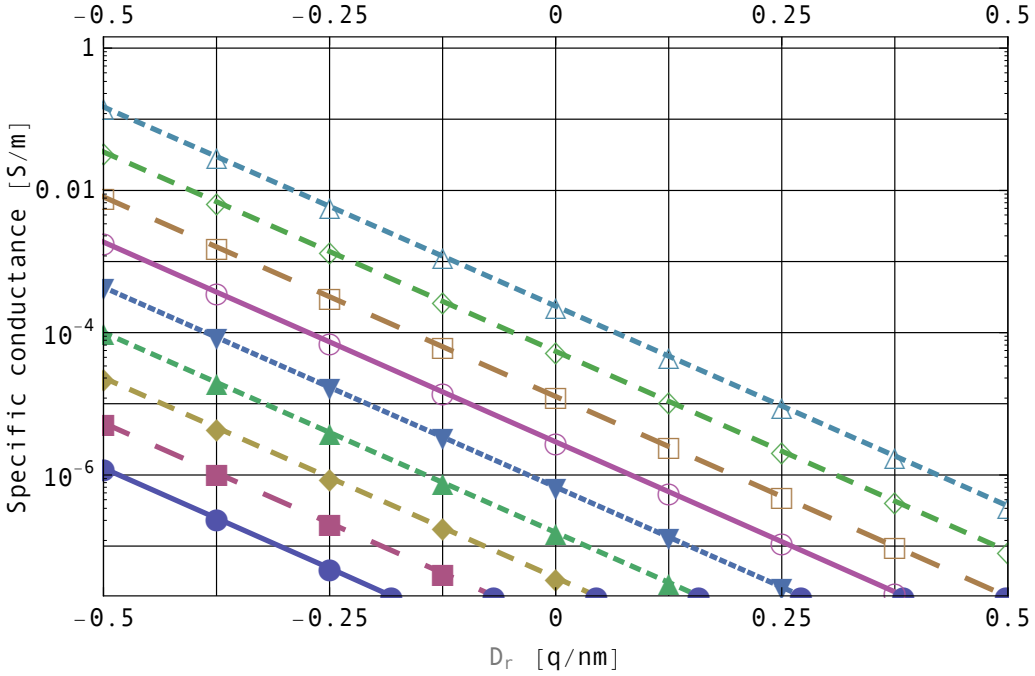

Figure 2. The specific conductance of a nanowire as a function of the dipole moment D_r for different values of the surface charge density C on a logarithmic scale. The first line (blue, solid line with solid circles at the bottom) is for $C = -0.5\mathrm{q} \cdot \mathrm{nm}^{-2}$; the last line (light blue, dashed line with hollow triangles at the top) is for $C = +0.5\mathrm{q} \cdot \mathrm{nm}^{-2}$; the lines in between correspond to steps of $0.125\mathrm{q} \cdot \mathrm{nm}^{-2}$. The liquid contains $10^{-6}\mathrm{mol} \cdot \mathrm{l}^{-1}$ of $\mathrm{Na}^{+}\mathrm{Cl}^{-}$; the nanowire is p-doped with $10^{16}\mathrm{q} \cdot \mathrm{cm}^{-3}$, it is 150nm long, the silicon core has a radius of 2nm, and the silicon-oxide layer has a thickness of 2nm.

layer. This argument supports the notion that a careful analysis of the charges in the boundary layer must be carried out. Therefore we quantify the influence of the dipole moment in the following simulations.

Figures 2, 3, and 4 show the specific conductances of nanowire sensors with a length of 150nm and with different diameters of 2nm, 6nm, and 10nm as a function of the dipole moment D_r. Several curves for different surface charge densities were simulated. They all show similar behavior, namely an exponential decrease in conductance for these devices as the dipole moment increases. This means that not only the total charge of the boundary layer modulates the conductance of the transducer, but that its dipole moment has significant influence as well. Furthermore, the magnitude of the slope of the conductance curves increases as the diameter of the nanowires decreases; as expected, thinner wires are better sensors.

Experiments with nanowire sensors show conductance changes from about 10% up to a factor of about 3, as mentioned above. As seen in the figures, a small change in dipole moment, in the vicinity of roughly $0.05\mathrm{q} \cdot \mathrm{nm}^{-1}$, yields a conductance change by a factor of about 3.

Therefore the boundary layer cannot be modeled only by including its total charge; the quantitative results show that its dipole moment must be considered as well to arrive at satisfying quantitative descriptions. The higher-order effect of the dipole moment of the boundary layer must be included in models and simulations of field-effect biosensors. Indeed, small changes in the dipole moment due to a reconfiguration of the charges in the boundary layer upon binding of target molecules may be the primary detection mechanism.

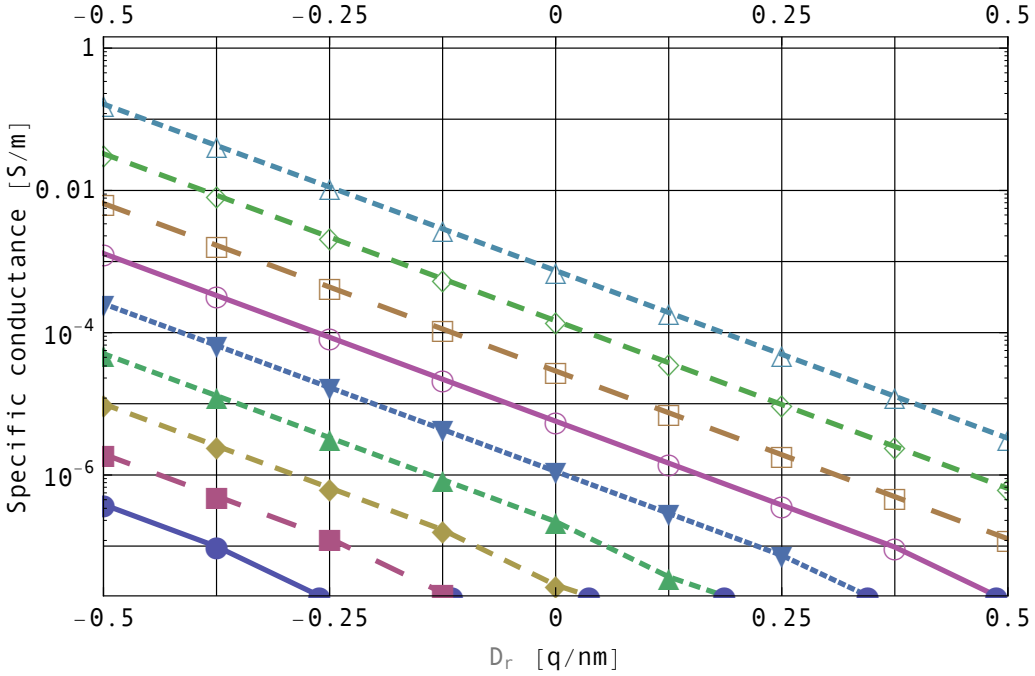

Figure 3. The specific conductance of a nanowire as a function of the dipole moment D_r for different values of the surface charge density C on a logarithmic scale. Here the silicon core has a radius of 6nm.

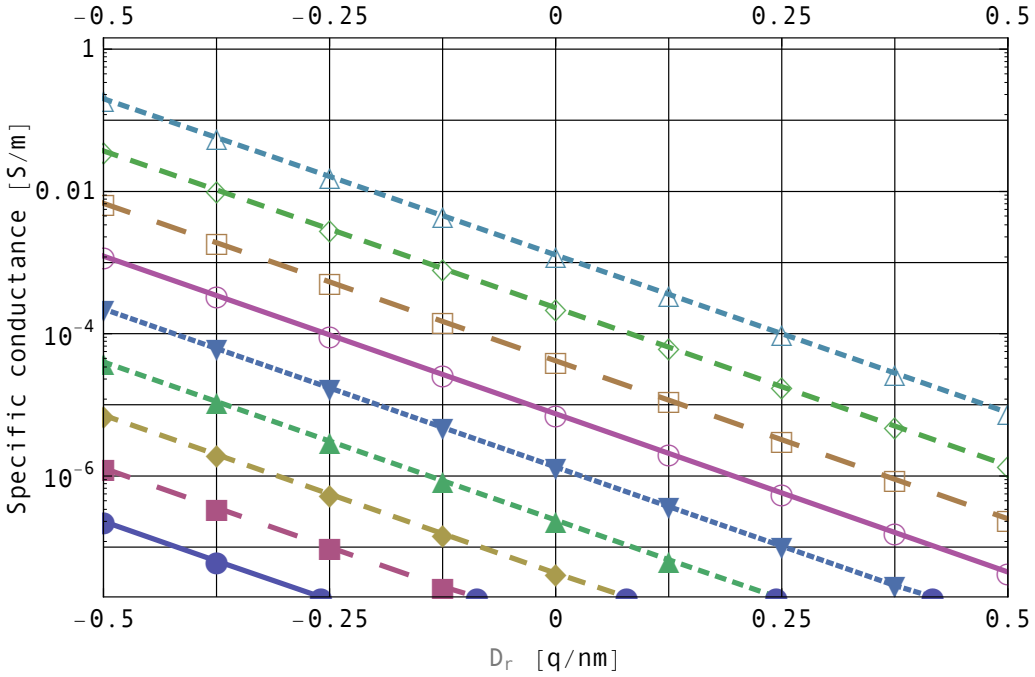

Figure 4. The specific conductance of a nanowire as a function of the dipole moment D_r for different values of the surface charge density C on a logarithmic scale. Here the silicon core has a radius of 10nm.

4. Deployment on the nanoHUB

We have developed a web interface for our simulator so that other researchers can access it via an ordinary web browser and perform their own simulations. Our tool is one of more than 60 tools available at `nanoHUB.org`, a cyber-infrastructure project created to support online simulation. To streamline the process of publishing tools, the nanoHUB team has developed a toolkit called RAPPTURE, which creates interactive graphical user interfaces automatically based on the description of a tool. The resulting interface can be used on the desktop or deployed on the web via the nanoHUB middleware.

4.1. The nanoHUB

The Network for Computational Nanotechnology (NCN) has created a resource for nano-science research and education, embodied by the web site `nanoHUB.org`. Over 5 900 users ran over 245 000 simulations in the year 2007. Overall more than 26 000 users interacted with the nanoHUB. Here a user is defined as a person identified by a login who ran at least one simulation, or a person identified by an IP address that had a continuous session of at least fifteen minutes on the nanoHUB.

The nanoHUB is more than just a repository; it offers integrated, online web meetings via Macromedia Breeze, source code collaboration through its nanoFORGE.org area, events calendars, and many other services designed to connect researchers and build a community. But most importantly, the nanoHUB connects users to the simulation tools they need for research and education. Users can access more than 60 interactive graphical tools, and not only launch jobs, but also visualize and analyze the results via any web browser. Simulation jobs can be dispatched on national grid resources, including the NSF TeraGrid and the Open Science Grid. The nanoHUB middleware hides much of the complexity of grid computing, handling authentication, authorization, file transfer, and visualization, and lets the user focus on research, education, or learning.

4.2. The RAPPTURE *toolkit*

Many simulation tools are driven by a control file of some sort, which contains parameter settings and other details about the simulation, along with the names of various data files describing the input structure. In order for such a tool to be published on the web, an interface must be created to query the various parameters, collect the input files, launch the tool, and present the results. This interface is slightly different for each tool, and involves a lot of customized coding. This can be done in a variety of web programming languages, but when done in this manner, the resulting interface can be used only through a web browser. A casual user who is introduced to a tool through the web is completely lost when faced with the command file interface for the same tool on the desktop. So it is often difficult for casual users to make the transition to become power users.

Instead, we have taken a very different approach to tool development. We have created a toolkit called RAPPTURE (the Rapid Application Infrastructure) which streamlines the creation of Graphical User Interfaces (GUIs) for all simulation tools. RAPPTURE GUIs work the same way whether running locally on the user's desktop under Mac OS X, the X window system, or Microsoft Windows, when running remotely through the user's web browser through the nanoHUB middleware. RAPPTURE GUIs are created automatically with a minimum of effort by describing the input and output parameters associated with a tool as RAPPTURE objects in the Extensible Markup Language (XML).

Describing the inputs and outputs is the first half of the development process. The second half is writing the code within a simulator to access these elements. RAPPTURE has bindings for a variety of programming languages, including C/C++, Fortran, Python, Matlab, Perl, and Tcl, so scientists can use the RAPPTURE application programming interface naturally within their

favorite programming environment. Alternatively scripts written in Python, Tcl, or Perl can translate RAPPTURE objects into legacy code inputs and outputs without modifying the original science code.

The RAPPTURE GUI drives the whole interaction. There is one generic GUI program for all RAPPTURE tools. This program reads the XML description for a tool and produces the interface automatically on-the-fly using Tcl/Tk widgets. The user interacts with the GUI, enters values, and eventually presses the "Simulate" button. At that point, RAPPTURE substitutes the current value for each input parameter into the XML description, and launches the simulator with this XML description as the driver file. The simulator reads the inputs, computes the outputs, and sends the results back to the RAPPTURE GUI. The GUI then loads the results into the output analyzer for the user to explore.

The RAPPTURE toolkit makes it easy to add new parameters to a simulator. First the XML description of the simulator is updated and then the simulator source code is updated to access the new parameters. RAPPTURE generates the GUI dynamically each time a tool is invoked based on the information available at that point. As changes are made to a program, RAPPTURE detects the changes and adjusts the GUI accordingly the next time the tool is executed.

4.3. Middleware

When applications are invoked on the nanoHUB, they are controlled by a middleware system designed to project the graphical session to a user's web browser. To make this occur in a way that hides the details from the user, the middleware is responsible for a variety of operations. These operations include checking the user's authorization to use an application, setting up the user's filesystem, configuring firewall rules, starting the application with a proper configuration, projecting the graphical session through VNC, terminating the application upon lengthy inactivity, and collecting the statistics of the application.

Our requirements for middleware were derived from experience with the In-VIGO [28] and PUNCH [29] middleware systems. Both employ virtual file systems to map user requests to applications running in shadow accounts on execution hosts. They also use HTML form-based input to direct the operations of command-line tools, with graphical interaction happening as a side-effect. Two items provided the motivation to create a simplified middleware system. The first was the need to more easily support graphical applications as first-class entities. The second was the desire to leverage features already available in the native operating system such as file system quotas and interactive session support. The resulting middleware deals more directly with the base system by no longer using virtual file systems or shadow accounts.

The middleware team has deployed two new generations of middleware since PUNCH and In-VIGO, namely Narwhal and Maxwell. Details of the middleware developments can be found online [30]. Narwhal provided significant improvements over In-VIGO in terms of reduction of number of code lines (due to the move from Java to scripting languages), system speed, reliability, automatic failure recovery, and testability. The next generation middleware represented a shift in philosophy from a middleware system that allocates resources to one that regulates access between systems and between zones of security. This is similar in spirit to Maxwell's demon, a thought experiment where a hypothetical shutter regulates the movement of molecules between two chambers. Furthermore the use of the term demon was already prevalent in the vernacular of software system architecture. Therefore the name Maxwell was selected.

5. Conclusion

Field-effect biosensors based on planar structures and nanowires have been fabricated in recent experiments. Their main advantage is label-free operation. Their functioning is believed by experimentalists to be due to a field effect [27], although a quantitative theory and understanding of their functioning has been missing. Since the devices rely on a field effect, a self-consistent

model of all the charges in the system, namely in the semiconductor, in the biofunctionalized layer, and in the liquid is necessary. Clearly the biofunctionalized layer is of crucial importance for the understanding of the devices.

We have developed multi-scale models that make it possible to bridge the differing length scales of the biomolecules in the biofunctionalized layer and the sensor dimensions. They are based on the solution of homogenization problems and mean that the biofunctionalized layer can be replaced by interface conditions. The interface conditions depend on the surface charge density and the dipole moment density of the biofunctionalized layer. Hence the multi-scale models provide the instrument to include the charge distribution of the biofunctionalized boundary layer in self-consistent simulations.

Using this model, we have performed conductance simulations of realistically sized nanowire sensors with different diameters using the drift-diffusion model as the charge transport kernel in order to investigate the influences of the surface charge density and the dipole moment density of the boundary layer. Numerical evidence was found that the dipole moment density of the boundary layer affects the conductance of the transducer exponentially. Therefore simpler models including only the total charge of the boundary layer are not sufficient. Another conclusion is that a change in the dipole moment of the boundary layer, i.e., a reconfiguration of the partial charges of the biomolecules and of the ions near the biomolecules and in the electric double layer, may be the primary field-effect detection mechanism.

Acknowledgment

The authors thank Dieter Baurecht, Alena Bulyha, Heidrun Karlic, Christoph Überhuber, and Franz Varga for discussions. We also thank Edward Howell and Steven Clark for their assistance in developing and testing the web interface.

This work was supported by the Austrian Ministry of Science via its grant for the Wolfgang Pauli Institute and by the EU project DEASE (contract MEST-CT-2005-021122). C.R.'s work was supported by National Science Foundation award no. DMS-0718308. At Purdue work was supported by the National Science Foundation, the Indiana 21st Century fund, and the Semiconductor Research Corporation. nanoHUB.org computational resources were used in this work.

References

[1] P. Bergveld. Development of an ion-sensitive solid-state device for neurophysiological measurements. *IEEE Trans. Biomed. Eng.*, BME-17:70–71, 1970.

[2] P. Bergveld. Development, operation and application of the ion sensitive field effect transistor as a tool for electrophysiology. *IEEE Trans. Biomed. Eng.*, BME-19:342–351, 1972.

[3] P. Bergveld and A. Sibbald. *Analytical and Biomedical Applications of Ion-Selective Field-Effect Transistors*. Elsevier, Amsterdam, 1988.

[4] M.J. Schöning and A. Poghossian. Recent advances in biologically sensitive field-effect transistors (BioFETs). *Analyst*, 127:1137–1151, 2002.

[5] A. Poghossian, A. Cherstvy, S. Ingebrandt, A. Offenhäuser, and M.J. Schöning. Possibilities and limitations of label-free detection of DNA hybridization with field-effect-based devices. *Sensors and Actuators B*, 111-112:470–480, 2005.

[6] M.J. Schöning and A. Poghossian. Bio FEDs (field-effect devices): State-of-the-art and new directions. *Electroanalysis*, 18(19-20):1893–1900, 2006.

[7] E. Souteyrand, J.P. Cloarec, J.R. Martin, C. Wilson, I. Lawrence, S. Mikkelsen, and M.F. Lawrence. Direct detection of the hybridization of synthetic homo-oligomer DNA sequences by field effect. *J. Phys. Chem. B*, 101:2980–2985, 1997.

[8] J. Fritz, E.B. Cooper, S. Gaudet, P.K. Sorger, and S.R. Manalis. Electronic detection of DNA by its intrinsic molecular charge. *Proc. Nat. Acad. Sci. U.S.A.*, 99(22):14142–14146, October 2002.

[9] J. Hahm and C.M. Lieber. Direct ultrasensitive electrical detection of DNA and DNA sequence variations using nanowire nanosensors. *Nano Lett.*, 4(1):51–54, 2004.

[10] Z. Li, Y. Chen, X. Li, T.I. Kamins, K. Nauka, and R.S. Williams. Sequence-specific label-free DNA sensors based on silicon nanowires. *Nano Lett.*, 4(2):245–247, 2004.
[11] Z. Li, B. Rajendran, T.I. Kamins, X. Li, Y. Chen, and R.S. Williams. Silicon nanowires for sequence-specific DNA sensing: Device fabrication and simulation. *Appl. Phys. A*, 80:1257–1263, 2005.
[12] G. Zheng, F. Patolsky, Y. Cui, W.U. Wang, and C.M. Lieber. Multiplexed electrical detection of cancer markers with nanowire sensor arrays. *Nature Biotechnology*, 23:1294–1301, October 2005.
[13] F. Patolsky, G. Zheng, and C.M. Lieber. Fabrication of silicon nanowire devices for ultrasensitive, label-free, real-time detection of biological and chemical species. *Nature Protocols*, 1(4):1711–1724, 2006.
[14] E. Stern, J.F. Klemic, D.A. Routenberg, P.N. Wyrembak, D.B. Turner-Evans, A.D. Hamilton, D.A. LaVan, T.M. Fahmy, and M.A. Reed. Label-free immunodetection with CMOS-compatible semiconducting nanowires. *Nature*, 445:519–522, February 2007.
[15] Clemens Heitzinger and Gerhard Klimeck. Investigation of conventional DNAFETs for genome-wide detection of polymorphisms. In *Proc. Eurosensors XX 2006*, volume 1, pages 448–449, Göteborg, Sweden, September 2006.
[16] Edward Howell, Clemens Heitzinger, and Gerhard Klimeck. Investigation of device parameters for field-effect DNA-sensors by three-dimensional simulation. In *Proc. IEEE Nanotechnology Materials and Devices Conference (NMDC 2006)*, volume 1, pages 154–155, Gyeongju, Korea, October 2006. IEEE.
[17] Clemens Heitzinger and Gerhard Klimeck. Computational aspects of the three-dimensional feature-scale simulation of silicon-nanowire field-effect sensors for DNA detection. *Journal of Computational Electronics*, 6(1-3):387–390, 2007.
[18] Sriraman Damodaran, Selvakumaran Vadivelmurugan, Quoc-Thai Do, Clemens Heitzinger, Yang Liu, Robert Dutton, and Gerhard Klimeck. Investigation of the conductance of silicon nanowire biosensors using the 2D drift-diffusion model. In *Proc. 10th NSTI Nanotech Conference 2007 (NSTI Nanotech 2007)*, pages 1374/1–3, Santa Clara, CA, USA, May 2007.
[19] Clemens Heitzinger, Christian Ringhofer, and Siegfried Selberherr. Investigations of the potential jump at the surface of BioFETs using a multi-scale model. In *Proc. 211th Meeting of the Electrochemical Society (ECS)*, page 947, Chicago, IL, USA, May 2007. The Electrochemical Society.
[20] Clemens Heitzinger. Modeling BioFETs, an emerging nano-biosensor technology, October 2007. Workshop on Ion Channels (Special Semester on Quantitative Biology Analyzed by Mathematical Methods) at RICAM, Linz, Austria. *Invited.*
[21] Clemens Heitzinger, Norbert Mauser, and Christian Ringhofer. Homogenized interface conditions for multi-scale modeling of field-effect biosensors by the Poisson–Boltzmann equation. *Submitted for publication.*
[22] Clemens Heitzinger, Norbert Mauser, and Christian Ringhofer. Multi-scale modeling of nanowire field-effect biosensors. *In preparation.*
[23] P. Debye and E. Hückel. Zur Theorie der Elektrolyte. I. Gefrierpunktserniedrigung und verwandte Erscheinungen. *Physikalische Zeitschrift*, 24(9):185–206, 1923.
[24] C. Tanford. *Physical Chemistry of Macromolecules.* John Wiley & Sons, New York, NY, 1961.
[25] M.J. Holst. *The Poisson–Boltzmann Equation.* PhD thesis, University of Illinois at Urbana-Champaign, Urbana-Champaign, IL, USA, 1994.
[26] P.A. Markowich, C.A. Ringhofer, and C. Schmeiser. *Semiconductor Equations.* Springer-Verlag, Wien, 1990.
[27] Z. Gao, A. Agarwal, A.D. Trigg, N. Singh, C. Fang, C.-H. Tung, Y. Fan, K.D. Buddharaju, and J. Kong. Silicon nanowire arrays for label-free detection of DNA. *Analytical Chemistry A*, 79(9):3291–3297, 2007.
[28] S. Adabala, V. Chadha, P. Chawla, R. Figueiredo, J.A.B. Fortes, I. Krsul, A. Matsunaga, M. Tsugawa, J. Zhang, M. Zhao, L. Zhu, and X. Zhu. From virtualized resources to virtual computing grids: the In-VIGO system. *Future Generation Computing Systems*, 21(6), June 2005.
[29] N. H. Kapadia, R. J. Figueiredo, and J. A. B. Fortes. Enhancing the scalability and usability of computational grids via logical user accounts and virtual. In *Proceedings of the Heterogeneous Computing Workshop (HCW) at the International Parallel and Distributed Processing Symposium (IPDPS)*, pages 82–82, April 2001.
[30] The chronology of nanoHUB middleware. https://www.nanohub.org/about/middleware/.